Supplementary Figures

Beating the Heat - Fast Scanning Melts Silk Beta Sheet Crystals

Peggy Cebe[1*], Xiao Hu [2§], David L. Kaplan[2],

[1] Department of Physics and Astronomy, and [2] Department of Biomedical Engineering
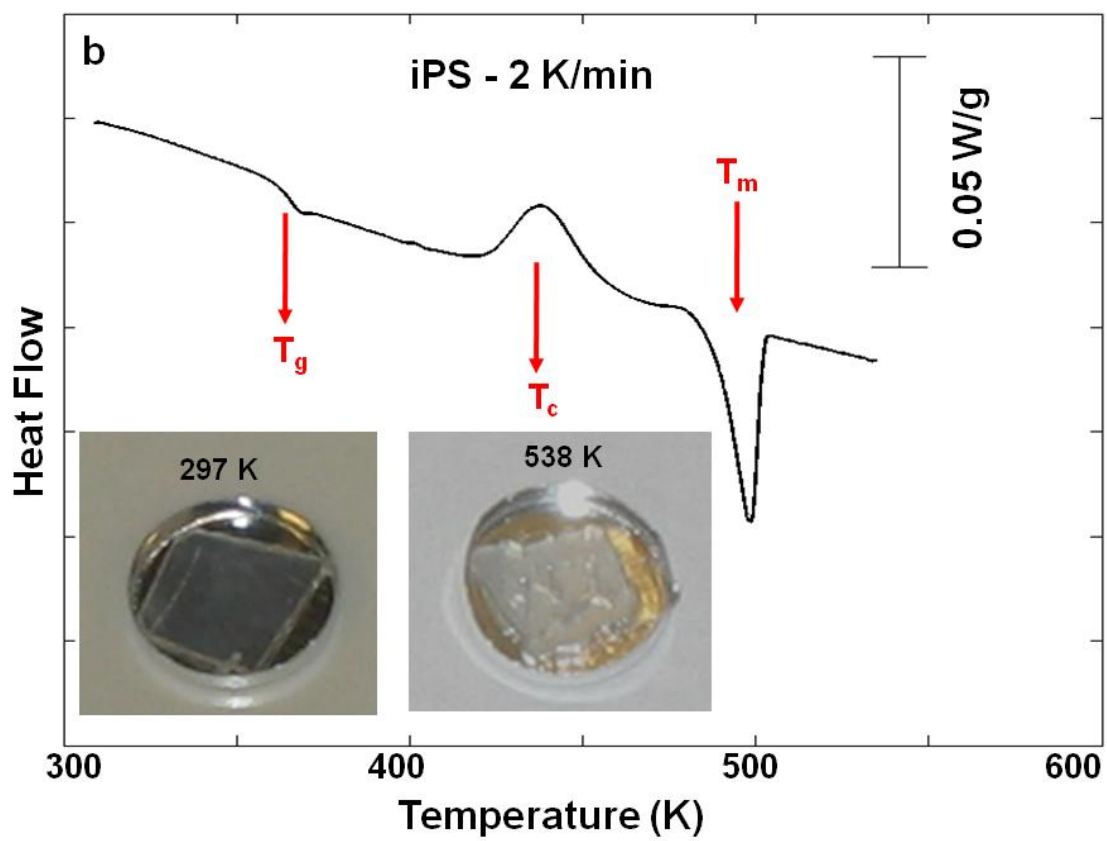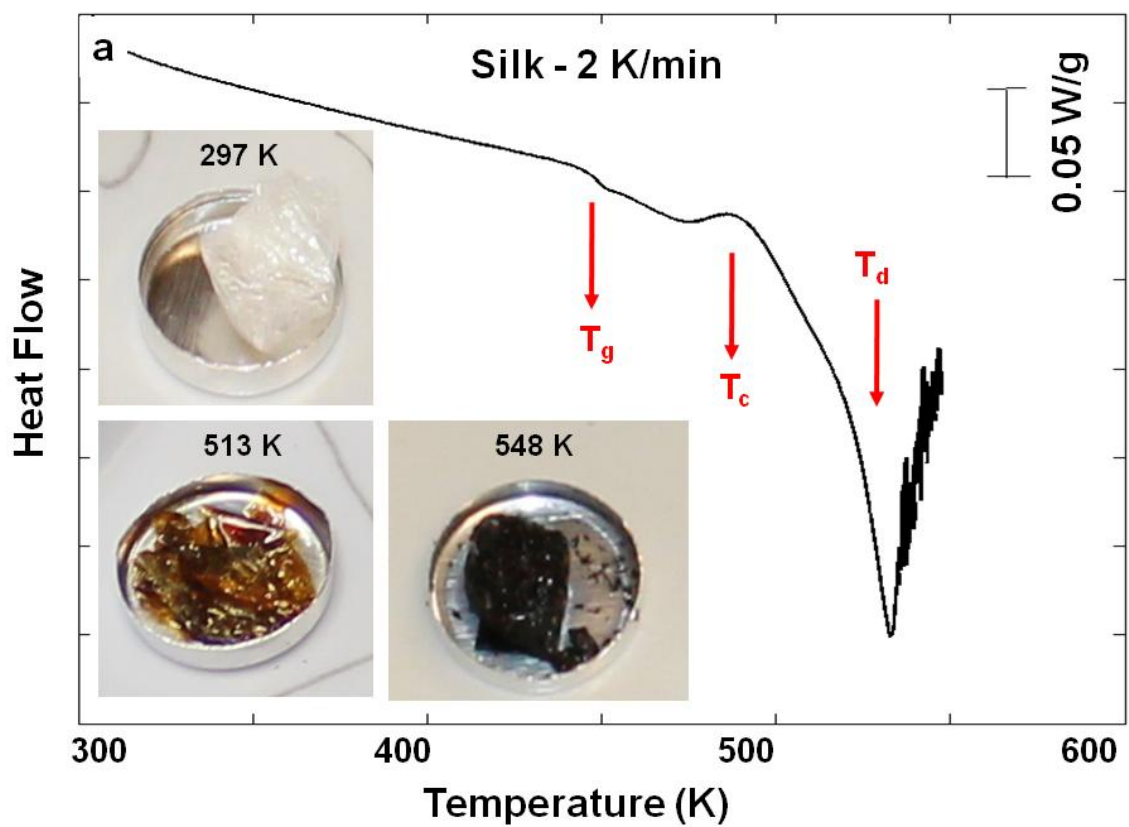
Tufts University, Medford MA, 02155, USA

Evgeny Zhuravlev, Andreas Wurm, Daniela Arbeiter[#], Christoph Schick[*]

Institute of Physics, University of Rostock, 18051 Rostock, Germany

* Contact Authors: peggy.cebe@tufts.edu, christoph.schick@uni-rostock.de

[§] Current Address: Department of Physics & Astronomy, and Department of Biomedical

Engineering and Sciences, Rowan University, Glassboro, NJ 08028, USA

[#] Current Address: Institute for Implant Technology and Biomaterials e.V., Rostock, Germany

a Silk - 2 K/min

0.05 W/g

Heat Flow

297 K

513 K

548 K

T_g

T_c

T_d

Temperature (K)

b iPS - 2 K/min

0.05 W/g

Heat Flow

T_m

T_g

T_c

297 K

538 K

Temperature (K)

Supplementary Figure S1. *Sample appearance and thermal traces at 2 K/min by conventional DSC for films of silk fibroin (a) and synthetic polymer (b), showing degradation peak of silk above 500 K. Images are taken at room temperature with the material inside an aluminum DSC pan (pan is ~7 mm in diameter), after the film had been heated to the temperature indicated. Observed transitions include the glass transition (T_g), crystallization (T_c), melting (T_m) and degradation (T_d). All DSC tests are conducted under an inert nitrogen gas atmosphere.*
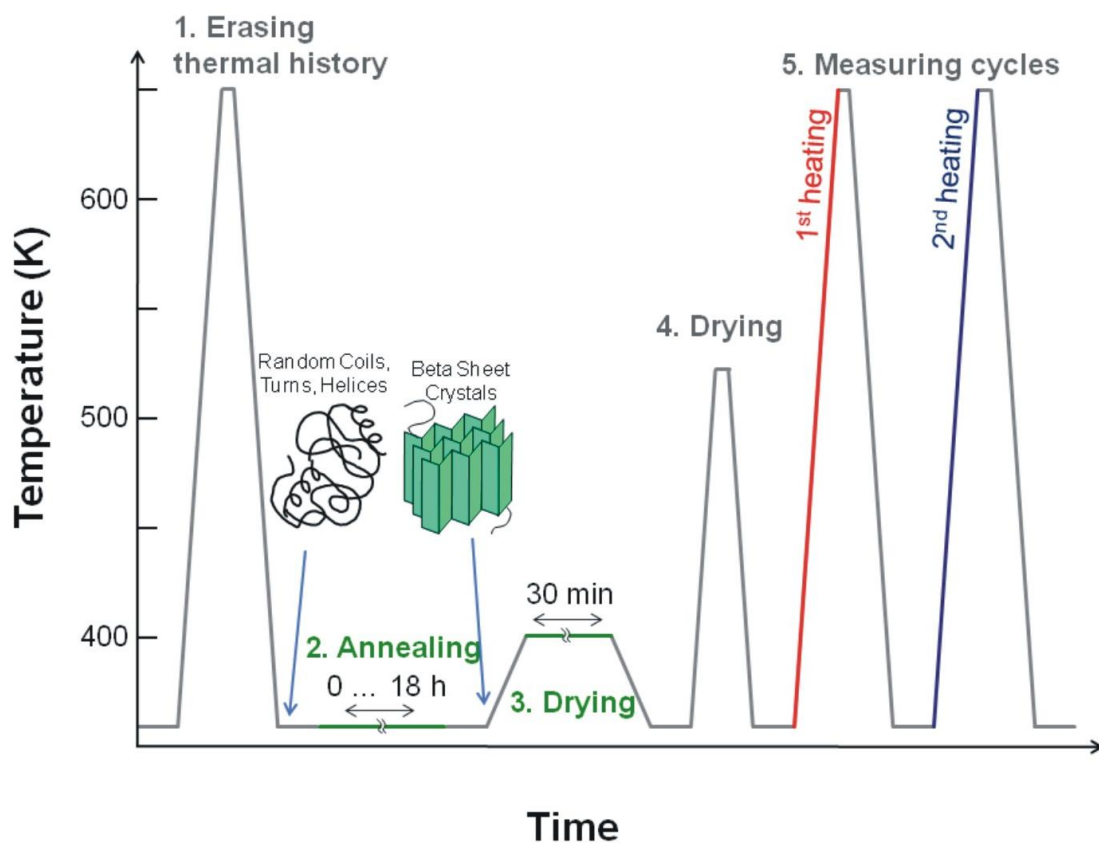
Supplementary Figure S2. *Complete sequence of sample treatments: 1. Heating from 360 K to 650 K to erase prior thermal history. 2. Crystallization by exposure to hot water vapor or methanol. 3. Drying at 430 K to remove bound water. 4. Heating above T_g to 520 K to remove enthalpy relaxation effects caused by step 3 and any remaining water or residual MeOH. 5. Measuring cycles involve rapid heating and cooling from 360 K to 650 K at 2,000 K/s, while heat flow data are recorded.*
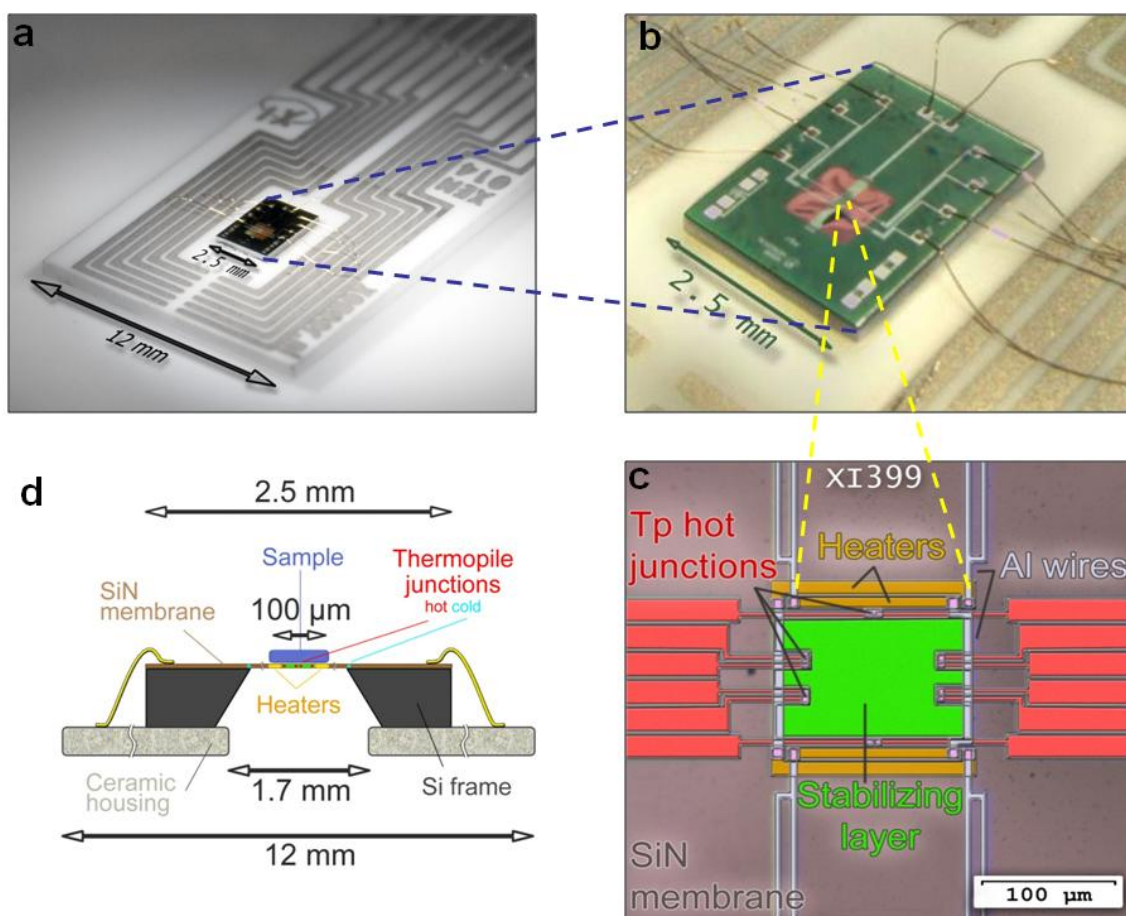
**Supplementary Figure S3.** *The Fast Scanning Chip Calorimeter Sensor. Clockwise from upper left: Images of the sensor XI399 (a, b) at different magnifications. Schematic of the central portion of the sensor (c) and cross section of the components (not to scale) (d). The silk sample is placed on the SiO_2 covered SiN_x membrane just on the thermal conducting layer of doped polysilicon (shown in green in c, d).*
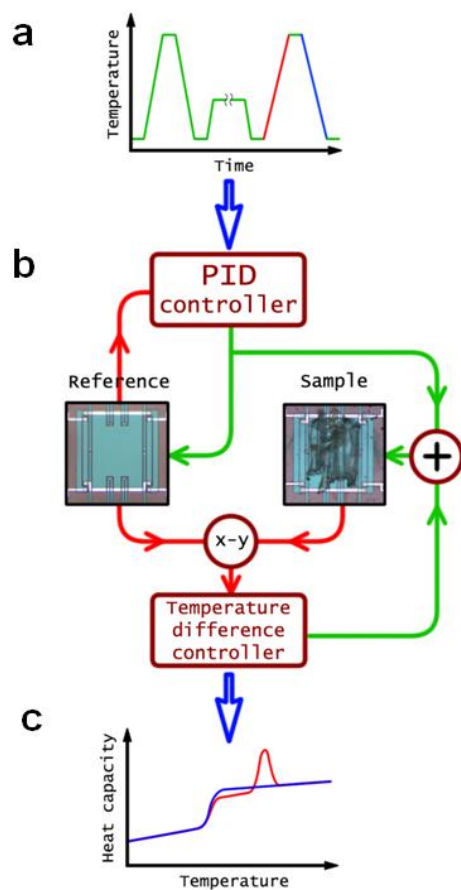
**Supplementary Figure S4.** *Scheme of the power compensated fast scanning calorimeter. The temperature profile is generated by the user and is provided to the PID controller through a DAC board (a). Reference and sample temperature follow the required profile by means of control loops (b). The resulting temperature difference can be recalculated to heat flow rate and sample heat capacity as shown in the scan at the bottom (c).*
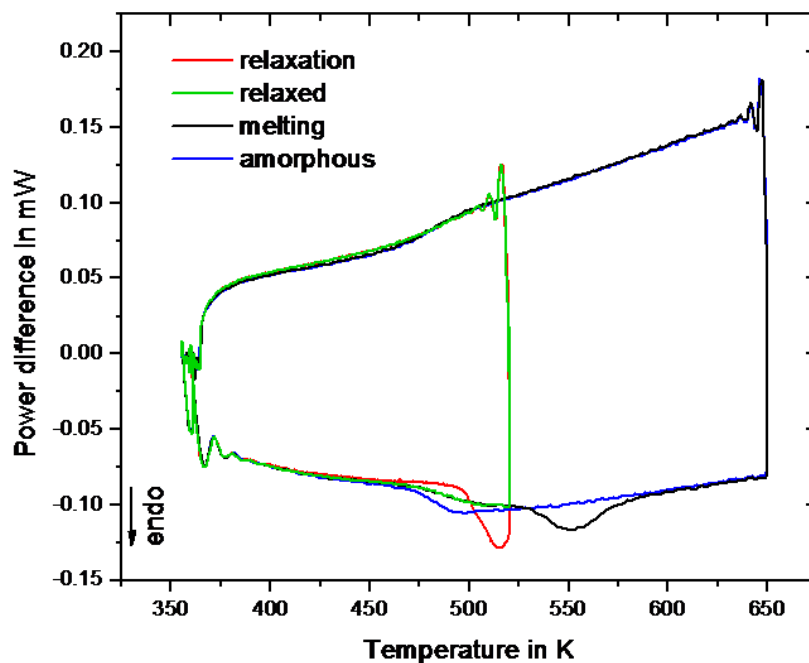
Supplementary Figure S5. *Power difference on heating and cooling, measured according the scheme in Supplementary Figure S2 after drying. The black curve corresponds to process step 4 - Relaxation. The green curve shows a subsequent repetition of the relaxation cycle for validation of successful relaxation. Red and blue lower curves correspond to process step 5 - Measuring cycles, 1ˢᵗ heating and 2ⁿᵈ heating, respectively. The upper red and blue curves are the cooling data after the first and second heating.*
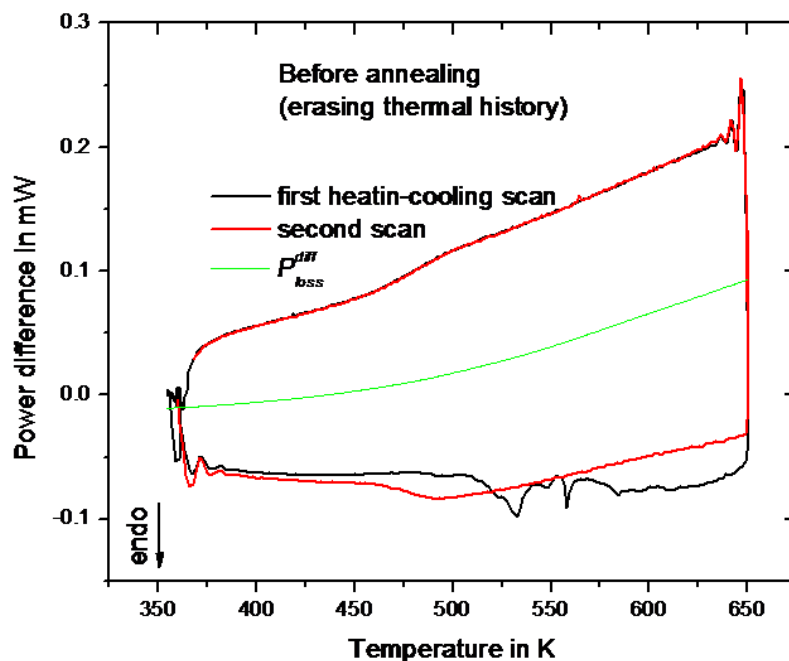
Supplementary Figure S6. *Power difference upon heating and cooling of a freshly prepared sample (black) and the subsequent reheating run (red). The green line corresponds to the symmetry line for correction of the heat loss difference, $P_{loss}^{diff}(T)$. During the first scan above T_g (black) a good thermal contact between sample and sensor is established. The changing contact and evaporating solvent residues cause the erratic behavior of the curve, which is not seen in the successive scans.*
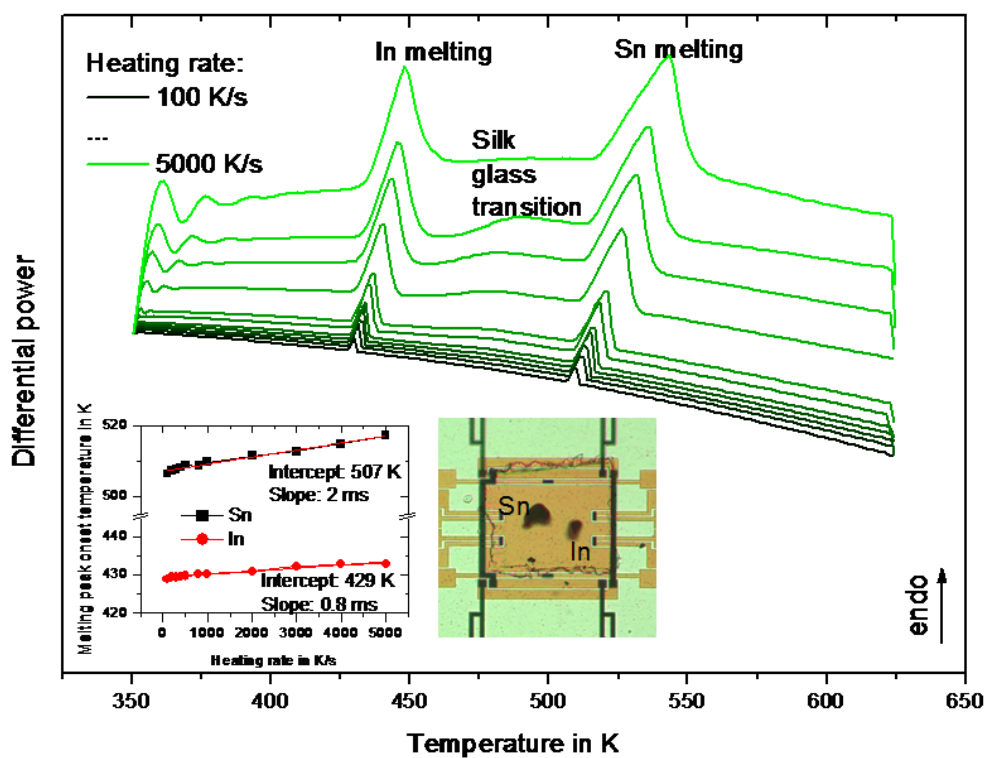
Supplementary Figure S7. *Heating scans of indium and tin particles on top of a ca. 20 μm thick silk sample at heating rates between 100 K/s and 5,000 K/s for checking thermal lag and temperature calibration. The insets show a photograph of the sample arrangement and the heating rate dependence of the melting peak onset temperatures.*

9
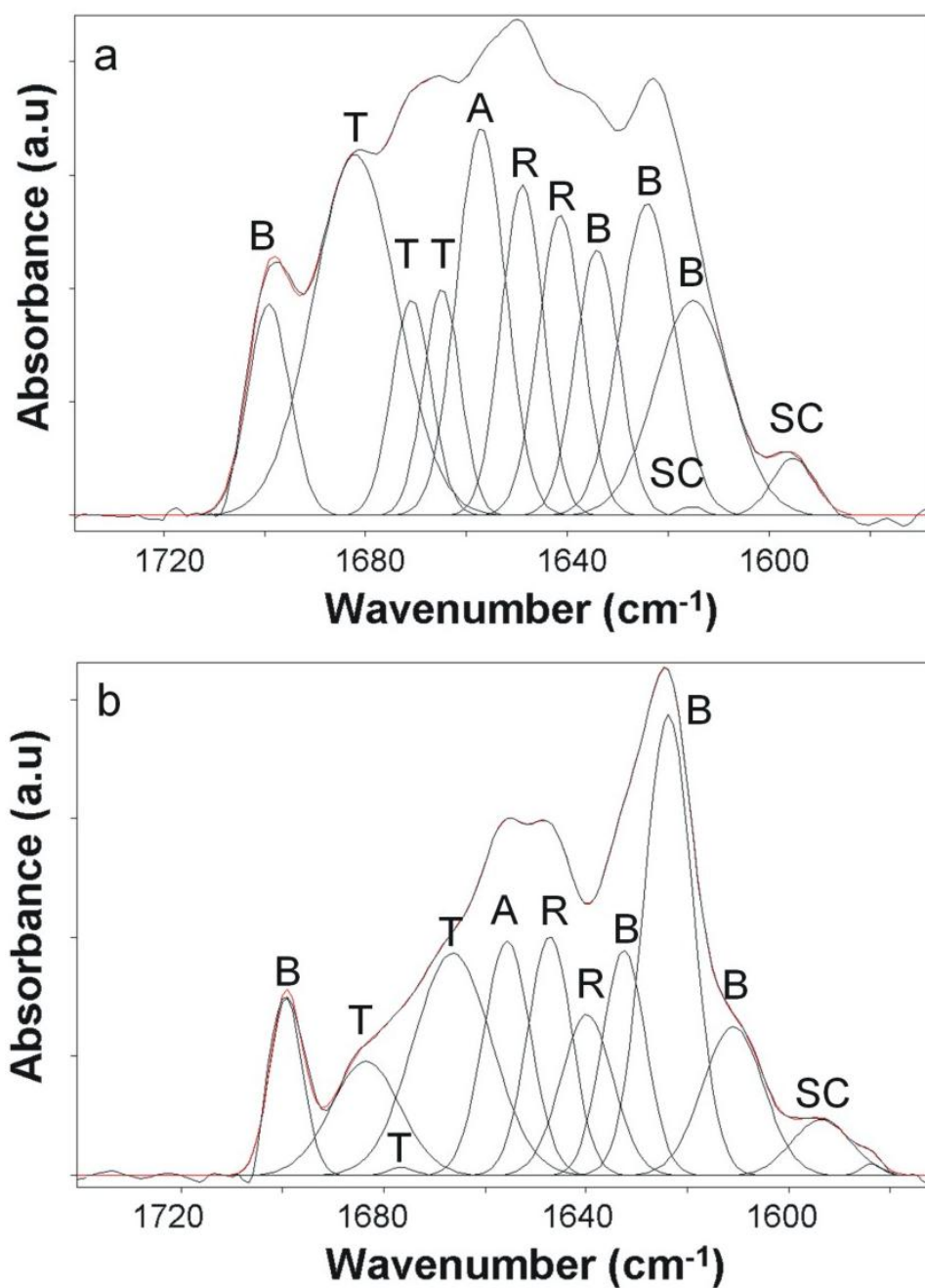
Supplementary Figure S8. *Illustration of the Fourier Self Deconvolution technique*[36, 37] *resulting in 12 fitting peaks marked as: B - beta pleated sheets crystals, T - turns, A - alpha helices, R - random coils, or SC - side chains. Peaks are referenced according to their assignments in the literature*[26, 27, 38-42]*. Degree of crystallinity is determined from the relative area of the four beta pleated sheet crystal peaks to the total absorbance spectrum. (a) Sample exposed to water vapor annealing, with crystallinity of 0.283 (Fig. 3c film); (b) Sample with crystallinity of 0.449 (Fig. 3c fibers).*

Supplementary Methods

Degradation Studies

Films were examined using conventional differential scanning calorimetry at a rate of 2 K/min, with heating in an inert nitrogen atmosphere. Silk fibroin was compared to a synthetic polymer, isotactic polystyrene (iPS). The DSC traces in **Supplementary Fig. S1** show that silk fibroin undergoes severe degradation, as illustrated by the large endothermic peak marked T_d. The silk begins to lose mass during this thermal event, and loses contact with the DSC aluminum pan causing erratic signal above 530 K. In contrast, the synthetic polymer heated at the same rate exhibits a melting endotherm in **Supplementary Fig. S1**, and no degradation when heated up to 530 K.

Images of exemplars at room temperature are shown in the insets of **Supplementary Fig. S1,** after heating up to different temperatures with the sample resting inside the aluminum DSC pan. At 297 K, before heating, both silk fibroin and iPS films were transparent. When silk fibroin is heated at 2 K/min to 513 K, the films begin to degrade[18], and become brown. Further heating to 548 K causes the silk fibroin to degrade to black char. The iPS polymer experiences no degradation over this temperature range, and experiences some shape change due to melting. The iPS becomes opaque (appearing as white) because it crystallizes during cooling from the molten state. Thermal degradation, at temperatures lower than the melting temperature, is also typical of some synthetic polymers, *viz.*, those possessing rigid molecular chains, such as polyparaphenylene terephthalamide (Kevlar[TM])[43], but is not typical of flexible chain polymers, such as iPS.

Fast Scanning Calorimeter data recalculation and temperature calibration

The user defined time-temperature profile, **Supplementary Fig. S4** (panel a), is recalculated into a voltage and provided as the set-point for the PID controller. The PID controller (panel b) makes the temperature of the reference sensor (which is empty of sample),

see **Supplementary Fig. S3** for details, to follow the experimental profile by adjusting power P_0 to its heater. The same power P_0 is applied to sample loaded sensor. The difference between the temperatures of reference and sample side is minimized by the differential controller by adding a power P_{diff} to the sample side.

The heat capacity of the sample during the scan can be recalculated from P_{diff} and heating rate using the heat balance equations

$$\text{reference:} \qquad C_0^{ref}\frac{dT^{ref}}{dt} = P_0^{ref} - P_{loss}^{ref}(T)$$

$$\text{sample:} \qquad (C_0^{sample} + C_{sample})\frac{dT^{sample}}{dt} = P_0^{sample} + P_{diff} - P_{loss}^{sample}(T)$$

and the difference of the two above equations:

$$C_{sample}\frac{dT}{dt} = P_{diff} - P_{loss}^{diff}(T),$$

where $P_{loss}^{diff}(T)$ is the difference between heat losses to the surrounding between sample and reference side, mainly introduced by the sample itself. Here it is assumed that the two sensors and the scan rates are identical, $C_0^{ref} = C_0^{sample}$ and $\dfrac{dT^{ref}}{dt} = \dfrac{dT^{sample}}{dt}$ (for details see [16]).

For a stable sample the differential heat loss is a function of temperature only, therefore it can be determined by heating and cooling the sample at the same rate and calculating the smooth symmetry line (green line in **Supplementary Fig. S6**). But as soon as the sample has different losses on heating and cooling (e.g. semi-crystalline on heating and amorphous on cooling), the symmetry line cannot be determined precisely, causing unavoidable uncertainty of heat capacity determination of the semi-crystalline sample. For this reason we did not further evaluate the heat capacity curves, e.g., we did not determine the step height at T_g or the peak area of the melting peaks, both of which are measures of crystallinity.

12

To ensure that the temperature of the sample is determined correctly, tiny Indium and Tin particles were placed on top of a silk fibroin sample and melting of the metals was observed at different rates, see **Supplementary Fig. S7**. The melting peak onset temperatures on heating were used, as recommended for DSC, for temperature calibration. The onset temperature extrapolated to heating rate zero for Indium and Tin is 429 K and 507 K, respectively, which is in good agreement with the expected values of 429.7 K and 505.1 K[44]. The thermal lag at the top surface of the sample (slope of the heating rate dependence shown in the inset) does not exceed 2 ms confirming that the temperature gradient across the sample is less than 4 K at 2000 K/s.

Fourier Transform Infrared Spectroscopic Analysis

Fourier Self-Deconvolution (FSD) of the infrared spectra covering the Amide I region (1595~1705 cm^{-1}) was performed by Opus 5.0 software. The second derivative was first applied to the original spectra in the Amide I region with a nine-point Savitsky-Golay smoothing filter. Deconvolution was performed using Lorentzian lineshape with a half-bandwidth of 25 cm^{-1}, and a noise reduction factor of 0.3 (the fraction of the interferogram to which the combination of the deconvolution and apodization is applied). Apodization with a Blackman-Harris function was always performed automatically at the same time in the software.

The parameters were chosen based on the resolution and the band position of the deconvoluted spectra. The positions (in cm^{-1}) of the band maxima in the deconvoluted spectra were made to correspond to the frequency of the minima in the second derivative of the undeconvoluted spectra. The deconvoluted spectrum is better suited for subsequent curve-fitting[26,27,38], for example, by keeping the position of the bands stable when using the autofit program in the software, and by separating the Amide I region from the total deconvoluted spectra for making baseline correction. A straight baseline passing through the deconvoluted

Amide I spectra was subtracted. A baseline correction using the Bezier function was also made on the left and right sides of the deconvoluted Amide I region.

In order to measure the relative areas of the Amide I components, FSD spectra were then curve-fitted. The decomposition method assumes that the extinction coefficient for the C=O stretch vibration is same for the different structural components. Thus, band intensities are proportional to the fraction of each secondary structural component. The number and position (in cm^{-1}) of the fitted bands were taken from the smoothed second derivative of the original spectra.

Gaussian line shape profiles were used in the fit although the Voigt function (a convolution of Lorentzian and Gaussian functions) can also be used. Comparison of the fitting results shows that these two peak functions yield almost the same results in this study and the Lorentzian contribution to the band shape of the Voigt function was always less than 10% for the few non 100%-Gaussian contributed Voigt peaks after using autofit in the software. The curve-fitting proceeded as follows: (i) The initial band positions were fixed first, using a fixed number of the bands, but allowing their widths and heights to vary; (ii) The band positions were then allowed to change within a limited region by using the Levenberg-Marquardt algorithm; (iii) A nonlinear least-squares method was finally used to make the reconstituted overall curve as close as possible to the original deconvoluted spectra. The fitting results were further evaluated by examining the residual from the difference between the fitted curve and the original curve.

Finally, the deconvoluted Amide I spectra were area-normalized (see examples in **Supplementary Fig. S8**). The relative areas of the single bands were used to determine the fraction of the secondary structural elements as described in our prior work[16]. To avoid possible artifacts arising from the deconvolution step, we chose different FSD factors (*i.e.,* half-bandwidth = 15, 20, 30 cm^{-1} and noise reduction factor = 0.2, 0.4) for each spectrum. To evaluate the impact of different choices of FSD factors, we fitted the deconvoluted spectra,

using the curve fitting procedure above. Results showed very little difference for the fractions of the secondary structures.

References

38   Rheinstadter, M. C., Schmalzl, K., Wood, K. & Strauch, D. Protein-protein interaction in purple membrane. *Phys. Rev. Lett.* **103**, 128104-128104 (2009).

39   Dong, A., Huang, P. & Caughey, W. S. Protein secondary structures in water from second-derivative amide I infrared spectra. *Biochemistry* **29**, 3303-3308 (1990).

40   Mouro, C., Jung, C., Bondon, A. & Simonneaux, G. Comparative fourier transform infrared studies of the secondary structure and the CO heme ligand environment in cytochrome P-450cam and cytochrome P-420cam. *Biochemistry* **36**, 8125-8134 (1997).

41   Tretinnikov, O. N. & Tamada, Y. Influence of casting temperature on the near-surface structure and wettability of cast silk fibroin films. *Langmuir* **17**, 7406-7413 (2001).

42   Taddei, P. & Monti, P. Vibrational infrared conformational studies of model peptides representing the semicrystalline domains of Bombyx mori silk fibroin. *Biopolymers* **78**, 249-258 (2005).

43   Wunderlich, B. Thermodynamic description of condensed phases. *J. Therm. Anal. and Calorimetry* **102**, 413-424 (2010).

44   Sarge, S. M. *et al.* Metrologically based procedures for the temperature, heat and heat flow rate calibration of DSC. *J. Therm. Anal.* **49**, 1125-1134 (1997).